Investigation of spherical aberration effects on coherent lidar performance

Hu, Qi; Rodrigo, Peter John; Iversen, Theis Faber Quist; Pedersen, Christian

Published in:
Optics Express

Link to article, DOI:
10.1364/OE.21.025670

Publication date:
2013

Document Version
Publisher's PDF, also known as Version of record

Investigation of spherical aberration effects on coherent lidar performance

Qi Hu,[1] Peter John Rodrigo,[1,*] Theis F. Q. Iversen,[2] and Christian Pedersen[1]

[1] *DTU Fotonik, Department of Photonics Engineering, Technical University of Denmark, Frederiksborgvej 399, 4000 Roskilde, Denmark*

[2] *Windar Photonics A/S, Helgeshøj Alle 16-18, 2630 Taastrup, Denmark*

[*] *pejr@fotonik.dtu.dk*

Abstract: In this paper we demonstrate experimentally the performance of a monostatic coherent lidar system under the influence of phase aberrations, especially the typically predominant spherical aberration (SA). The performance is evaluated by probing the spatial weighting function of the lidar system with different telescope configurations using a hard target. It is experimentally and numerically proven that the SA has a significant impact on lidar antenna efficiency and optimal beam truncation ratio. Furthermore, we demonstrate that both effective probing range and spatial resolution of the system are substantially influenced by SA and beam truncation.

OCIS codes: (280.0280) Remote sensing and sensors; (280.3640) Lidar; (280.3340) Laser Doppler velocimetry.

References and links

1. The final report of the EU FP6 project UPWIND, http://www.upwind.eu/
2. J. Mann, J. P. Cariou, M. Courtney, P. Parmentier, T. Mikkelsen, R. Wagner, P. J. P. Lindelöw, M. Sjöholm, and K. Enevoldsen, "Comparison of 3D turbulence measurements using three staring wind lidars and a sonic anemometer," Meteorol. Z. **18**, 135–140 (2009).
3. T. Fujii and T. Fukuchi eds. *Laser Remote Sensing* (CRC Press, 2005).
4. Y. Zhao, M. J. Post, and R. M. Hardesty, "Receiving efficiency of pulsed coherent lidars. 1: theory," Appl. Opt. **29**, 4111–4119 (1990).
5. R. G. Frehlich and M. J. Kavaya, "Coherent laser radar performance for general atmospheric refractive turbulence," Appl. Opt. **30**, 5325–5352 (1991).
6. B. J. Rye and R. G. Frehlich, "Optimal truncation and optical efficiency of an apertured coherent lidar focused on an incoherent backscatter target," Appl. Opt. **31**, 2891–2899 (1992).
7. J. Y. Wang, "Optimal truncation of a lidar transmitted beam," Appl. Opt. **27**, 4470–4474 (1988).
8. B. J. Rye, "Primary aberration contribution to incoherent backscatter heterodyne lidar resturns," Appl. Opt. **21**, 839–844 (1982)
9. ZEMAX Optical Design Program User's Manual (July 8, 2011) pp. 196–199.
10. A. E. Siegman, "The antenna properties of optical heterodyne receivers," Appl. Opt. **5**, 1588–1594 (1966).
11. J. Mann, A. Peña, F. Bingöl, R. Wagner, and M. S. Courtney, "Lidar scanning of momentum flux in and above the atmospheric surface layer," J. Atmos. Oceanic Technol. **27**, 959-976 (2010).

1. Introduction

One of the main considerations in the development of the wind industry is the metrology issues. Essentially, more cost efficient and accurate wind velocity and turbulence mapping systems are highly desired [1]. Since the traditional cup and sonic anemometers require meteorological

#194245 - $15.00 USD Received 24 Jul 2013; revised 3 Sep 2013; accepted 10 Oct 2013; published 21 Oct 2013

masts, a detailed turbulence mapping will require a tremendous amount of masts at different locations and heights. For this particular task the laser remote sensing (lidar) technology offers an attractive alternative [2]. In these systems, precise control of multiple lidar units are required in order to acquire the full 3D wind vectors with high a spatial resolution, which is determined by the overlap between the individual lidar weighting function that describes the spatial sensitivity and confinement along each beam direction.

Descriptions of various lidar system designs are well documented in the literature [3–7]. However, those are all theoretical treatments and focus mainly on diffraction limited system designs. A previous theoretical analysis did include the aberration effects [8], but only for a fixed degree of beam truncation at the exit aperture that is optimal for an aberration-free system. This work is dedicated to investigating the weighting function change under the influence of SA to provide an experimental counterpart of the theory proposed by Rye [8], and we will expand the analysis to include optimization of the beam truncation in the presence of SA. In practice, most lidar designs involve lens selection for the telescope or optical transceiver, which predominantly suffers from SA due to the difficulty in manufacturing lenses with SA-corrected surfaces especially for larger aperture sizes with short focal lengths. Furthermore, Rye showed numerically [8] that for equal degrees of coma, SA and astigmatism, the SA is found as the dominant contributor to the lidar signal reduction.

2. Experimental setup

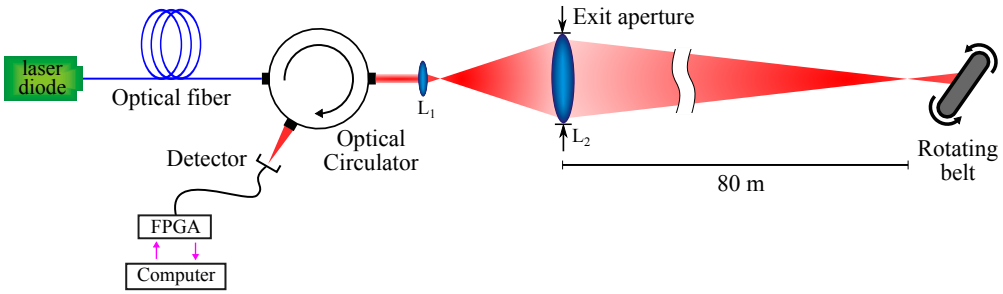

Fig. 1. Schematic layout of the system setup. The size of the exit aperture is the diameter of L_2. During the experiments several diffraction limited aspherical lenses, L_1 with different focal lengths are used in order to probe different ρ values; while two different L_2 are used to introduce different degree of aberrations. The rotating belt is used to generated the Doppler signal for our measurements.

In this work the impact of the SA is measured by probing the lidar weighting function of the system with a rotating belt as the hard target using a 1550 nm CW beam output as shown in the schematic layout in Fig. 1. Both the simulation and the experiment follows the geometry in Fig 1. The distance between L_1 and L_2 is adjusted such that the lidar signal is optimized with the hard target (rotating belt) placed at a range of 80 m. Around 0.5 mW of the diode laser output is tapped within the optical ciculator and is used as the local oscillator (LO) for the heterodyne detection. Both the signal from the rotating belt and the LO is focused onto the detector through the optical circulator. The ”virtual” back propagated local oscillator (BPLO) from the detector plane matches the transmit beam with a Gaussian field amplitude profile of radius, w, at the plane of lens L_2. This configuration is commonly referred to as the Wang design [7]. Different truncation ratios, $\rho = w/r_{L2}$ where r_{L2} is the radius of L_2 aperture, can be probed by changing the focal length (f_1) of lens L_1, since the imaging magnification of the

#194245 - $15.00 USD Received 24 Jul 2013; revised 3 Sep 2013; accepted 10 Oct 2013; published 21 Oct 2013

beam is dependent on the focal length ratio between L_1 and L_2. Two different L_2, both with exit aperture radius of $r_{L2} = 35.65$ mm (3 inch optics), are used in our experiments in order to evaluate the system under different degrees of SA. The lenses (L_2) are respectively a singlet lens ($f_2 = 200$ mm) that is not corrected for SA and a doublet lens ($f_2 = 216$ mm) designed for reduced SA. The correlation overview between the L_1 focal lengths and ρ can be found in Table 1. A quantitative illustration of the SA introduced by the L_2 lenses is shown in Fig. 2(a),

Table 1. Relation between focal lengths of L_1 and ρ

Focal length of L_1	4.6 mm	8.1 mm	11.3 mm	15.6 mm	18.8 mm
ρ, singlet lens	1.28	0.73	0.52	0.38	0.31
ρ, doublet lens	1.38	0.79	0.56	0.41	0.34

where the optical path difference (OPD) is measured in number of waves. The curves in Fig. 2(a) are generated using a Zemax simulation with monochromatic input, zero incident angle and assuming circular symmetry in the transverse plane, i.e. only the symmetrical components of wavefront errors are presented. The first six nonzero Zernike fringe coefficients, generated in Zemax, are listed in Table 2. Those coefficients are used to generate the OPD curves and they differ slightly from the standard Zernike coefficients, which is evident from the polynomials provided in the table. A detailed description of those coefficients can be found in the user's manual of Zemax [9]. It is evident from the table values that the SA (Z_9) is the dominant source of the waverfront errors.

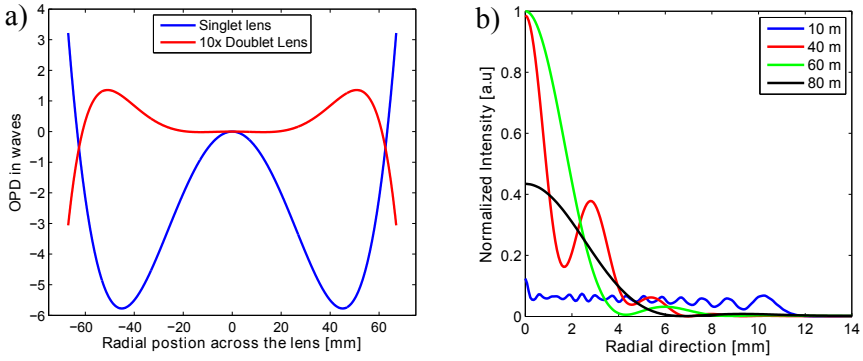

Fig. 2. a) The OPDs of the two different L_2 used in our experiments. The OPDs are generated in Zemax with zero incident angle and circular symmetry. b) The calculated transverse irradiance profile of the output beam in different axial distances from the singlet L_2. The focal length of L_1 is 15.6 mm in the simulation.

An accurate theoretical prediction of the field or irradiance distribution on the target side of L_2 is possible using those OPD curves. The SA can be incorporated in the theoretical simulation by introducing an extra phase term, ϕ_{SA} to the truncated Gaussian field at L_2 according to Eq. (1) [8]

$$E(r) = \begin{cases} E_0 \exp\left\{-\frac{r^2}{w^2} + i\phi(r) + i\phi_{SA}(r)\right\} & \text{for } 0 \le r \le r_{L2} \\ 0 & \text{for } r > r_{L2} \end{cases}, \quad \phi_{SA} = 2\pi * \mathrm{OPD}(r) \qquad (1)$$

where E_0 is the peak amplitude, r is the radial coordinate, $\phi(r)$ is the phase of the beam due

#194245 - $15.00 USD Received 24 Jul 2013; revised 3 Sep 2013; accepted 10 Oct 2013; published 21 Oct 2013

to field curvature, ϕ_{SA} is the phase term induced by the SA and the OPD(r) is either curves shown in Fig. 2(a). Due to the circular symmetry, the field on the target plane can be calculated numerically by a simple Fourier-Bessel transformation of Eq. (1) with an appropriate field curvature [8].

Table 2. Zernike fringe coefficients from Zemax

Term Z_j	Singlet L_2	Doublet L_2	Zernike fringe polynomials
Z_1	-3.27339159	0.03707405	1
Z_4	1.50844787	-0.05266555	$2p^2-1$
Z_9	4.87996531	-0.18513369	$6p^4-6p^2+1$
Z_{16}	0.10038714	-0.10019848	$20p^6-30p^4+12p^2-1$
Z_{25}	0.00231510	-0.00501370	$70p^8-140p^6+90p^4-20p^2+1$
Z_{36}	0.00005509	-0.00021833	$252p^{10}-630p^8+560p^6-210p^4+30p^2-1$

3. Results and discussions

To illustrate the degree of SA for the singlet L_2 case, the transverse irradiance profiles in different distances, z after the singlet L_2 are calculated and shown in Fig. 2(b). A side by side comparison between the numerical simulation and the experimental counterpart of the beam profiles is displayed in Fig. 3. The observed beam profiles are recorded with aid of an IR-detection card. An intensity clipping level was introduced in the presentation of the numerical results in order to simulate the saturation effect of the IR-detection card. In Fig. 3 the consistency between the simulations and the measurements is quite evident, qualitatively validating the accuracy of our theoretical simulations.

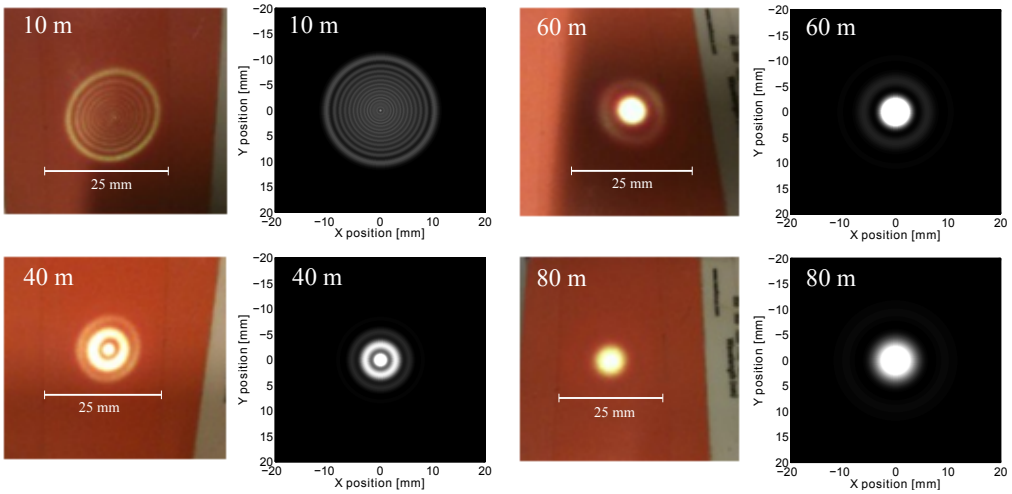

Fig. 3. The observed and simulated beam profiles emitted from the singlet L_2 in different axial distances (10m, 40m, 60m and 80m) The focal length of lens L_1 is 15.6 mm.

In order to maximize the signal in diffraction limited monostatic lidar systems, $\rho \approx 0.8$ through the L_2 is required [3]. However, in the presence of SA, optimal ρ will differ from

#194245 - $15.00 USD Received 24 Jul 2013; revised 3 Sep 2013; accepted 10 Oct 2013; published 21 Oct 2013

0.8 and the overall antenna efficiency will decrease compared to the aberration-free case. It is easiest to calculate the antenna efficiency, η_a using the target-plane formalism based on Siegman's antenna theorem [3, 10].

$$\eta_a(z) = \frac{\lambda^2 R^2}{A_r} \iint I^2_{\text{target}}(x,y,z)dxdy \tag{2}$$

where λ is the wavelength, R is the intended imaging or probing range (80 m in our case), A_r is the area of L_2 and I_{target} is the irradiance distribution of the output beam at the target plane position, z and is normalized by the total beam power before truncation.

In Fig. 4(a) the calculated antenna efficiency at $z = R$ as a function of ρ is shown for both L_2 lenses and compared with the aberration-free case (the dashed lines). The simulation is constructed such, that the algorithm is imitating the same distance optimization procedure as in the experiments. It is evident that not only the overall antenna efficiency has decreased as the consequence of SA, but the optimum ρ also shifts with different degrees of aberrations. Even for the doublet case where the SA is minimal, there is still a clear shift of the optimal ρ and a quite noticeable drop in the maximum antenna efficiency. It demonstrates the importance of considering the aberration effects in designing a lidar system. The result in Fig. 4(a) indicates that optimal ρ decreases with increasing degree of SA.

The measured hard target lidar signal as a function of ρ, normalized to the maximum data point of the doublet case, is also shown in Fig. 4(a). The experimental data shows the same tendencies as the numerical calculations. While the singlet data coincides quite well with the simulations, there is a slight deviation for the doublet case. Since the simulation only includes the SA effect, it is reasonable that the doublet data can deviate from the simulation due to other aberration effects in the rest of the system (we do observe small degree of astigmatism from the output of the optical circulator). The singlet data is, on the other hand, dominated by the SA, which explains the good agreement with the simulation.

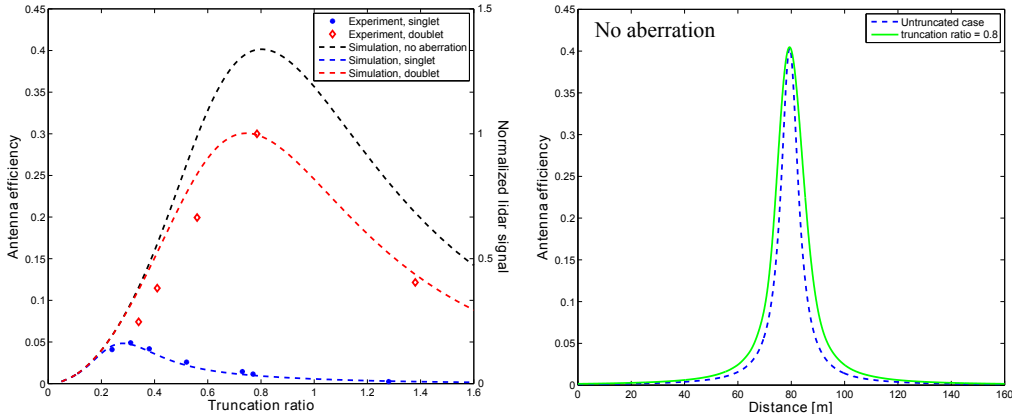

Fig. 4. a) The dash lines illustrates the numerically calculated antenna efficiency using Eq. (2) as a function of ρ; while the scattered points shows the measured lidar signal as a function of ρ. Both the simulation and the experimental data are acquired at a probing range of 80 m. b) The simulated antenna efficiency for the aberration-free case as a function of distance with and without the truncation effect ($\rho = 0.8$ for truncated case).

So far we have shown how the SA affects the optimal ρ with respect to the maximum antenna efficiency at fixed target distance equal to the intended probing range R. However, the graph in Fig. 4(a) only provides an optimal ρ for hard target case. For aerosol target, it is necessary

#194245 - $15.00 USD Received 24 Jul 2013; revised 3 Sep 2013; accepted 10 Oct 2013; published 21 Oct 2013

to analyze the lidar weighting function, which provides the effective probing range (may differ from R due to aberration), the spatial resolution and the total signal strength of the system. In a monostatic CW lidar the weighting function is commonly described by a Lorentzian function, F under the assumption of an ideal and untruncated Gaussian beam [11],

$$F = A\frac{1}{(z-R)^2+z_0^2} \tag{3}$$

where A is a normalization constant, z is the distance from L_2 and z_0 is the Rayleigh length of the output beam. However, we just demonstrated in Fig. 4(a) that a rather large ρ of around 0.8 is required in order to obtain the optimal antenna efficiency for the aberration-free system. In that case the output will suffer from significant diffraction effects due to the truncation and therefore no longer be considered as an ideal Gaussian beam. In Fig. 4(b) the antenna efficiency is calculated as a function of the distance for two different cases: 1) including the truncation effect by numerical integration of Eq. (2) and numerical Fourier-Bessel transform of the field in Eq. (1) to obtain I_{target}. 2) Using Eq. (3) based on the untruncated Gaussian beam assumption. The result demonstrates a broadening of the weighting function by 56% when including the truncation effect, which is quite significant. Since the width of this Lorentzian distribution is directly related to the spatial resolution of the lidar system, the truncation effect should not be underestimated in the system design.

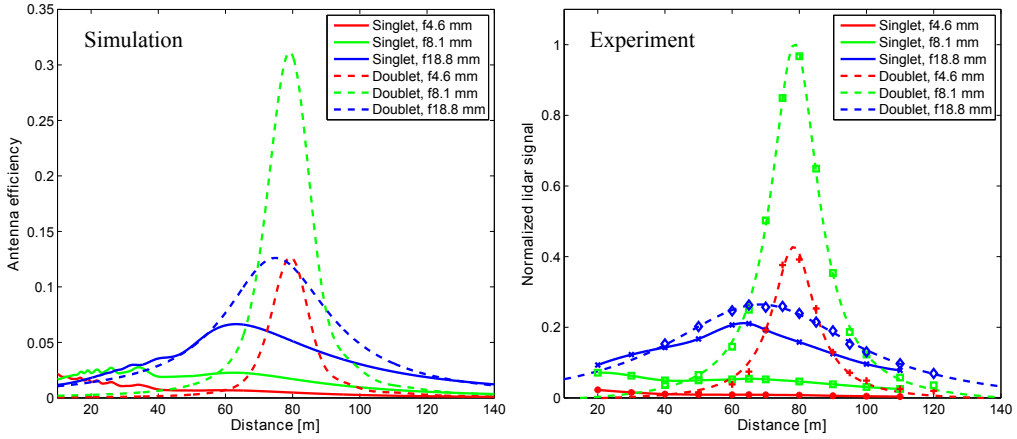

Fig. 5. The measured weighting functions for six different transceiver configurations along with their theoretical counterparts. The simulations are acquired using the numerical integration of the fields including the truncation diffraction effects. The blue solid line represents the optimal ρ of 0.3 for the singlet case, while the green dash line corresponds to the optimal ρ of 0.8 for the doublet case. The dash lines in the graph to the right are the Lorentzian fit to the experimental data (scattered points).

The weighting function can be acquired experimentally by measuring the lidar signal with a moving hard target. The experimental data of six different combinations of L_1 and L_2 are presented in Fig. 5 along with their numerical counterparts. In general the numerical results coincide quite well with the experimental data, but the singlet case gives a much better match than the doublet case. As we discussed earlier the simulations only include the SA effect, since the measurement with singlet L_2 is dominated by SA while the doublet L_2 case is not, it is expected that singlet lens case will provide a better fit. The simulation results do suggest that the full system (not only L_2) potentially suffers from other aberration effects like astigmatism and coma, which are comparable with the SA introduced by the doublet L_2, since the experimental

#194245 - $15.00 USD Received 24 Jul 2013; revised 3 Sep 2013; accepted 10 Oct 2013; published 21 Oct 2013

data shows a visible broadening of the weighting function compared with their numerical counterparts. Comparing the simulation with the experimental data there is a broadening of 21% for the green dash line ($f_1 = 8.1$ mm) while the broadening is 70% for the blue dash line case ($f_1 = 18.8$ mm). The residual broadening is likely due to the astigmatism of the beam from the optical circulator, which also explains the observed increase in the degree of broadening with the focal length of L_1.

From Fig. 5 it is quite obvious that in general one should reduce SA in the system, since both the spatial resolution/confinement and the maximum signal strength of the optimal doublet case (green dashed line) are much better than the optimal case for the singlet lens (blue solid line). However, the area under the weighting function (estimating the total lidar signal strength for aerosol target) has only increased by around 30% from the optimal singlet case to the doublet one. So for measurements of laminar air flow (i.e. negligible spatial dependence of wind vector), the benefit gained from using the more expensive doublet L_2 is minor in terms of signal strength enhancement but more on improved spatial resolution. For the more general turbulent air flow in the probing volume, higher signal strength enhancement due to tighter spatial confinement is of course expected.

From the previous theoretical treatments [8] we know that for a fixed ρ the weighting function will suffer from both peak shift and broadening effects under the influence of SA. Recalling Eq. (2) and the transverse irradiance profiles in Fig. 2(b) it is expected that the weighting function for the singlet L_1 case will have a peak around 60 m, since the effective beam confinement is tightest there and not at the intended imaging range, 80 m. The data shown in Fig. 5 provides, to our knowledge, the first experimental confirmation of these tendencies. But our numerical and experimental results also show that both the peak shift and the broadening effect can be compensated to certain degree by selecting a ρ appropriate for a particular degree of SA, which is not described in the theoretical work by Rye [8]. From the OPD curve in Fig. 2(a) we know that the doublet L_2 only suffers from minor SA, nevertheless, we still observe a weighting function peak shift of 2.4 m (for L_1 focal length of 8.1 mm), indicating the sensitivity of the lidar system to the SA effect. We also note in Fig. 5 that the peak shift is larger for lower ρ. Thus, in applications where delicate probing range control is necessary, it is advisable to calibrate the lidar system with a hard target by mapping the weighting function.

4. Conclusion

In this paper we have shown both numerically and experimentally that SA has a significant impact on antenna efficiency, optimal truncation ratio and the shape of the weighting function of a CW coherent lidar. If the system suffers from strong SA effect only very limited spatial confinement can be obtained as shown in Fig. 5. It is also evident that the degradation of spatial confinement or broadening of the lidar weighting function due to SA can be reduced by tuning the beam truncation through L_2. This corrective measure results from the novel finding in this work that the optimal truncation ratio depends on the degree of SA. Furthermore we have shown that both SA and truncation ratio influence the peak shift and width of the weighting function. In applications where precise probing range and spatial resolution are essential, a weighting function calibration of the lidar system using a hard target might be necessary. It is worth to stress that this study can also be applied to accurately model the weighting function of pulsed coherent lidar systems [2].

Acknowledgment

The authors would like to acknowledge the financial support from the Energiteknologisk Udviklings- og Demonstrations Program (EUDP) J.nr. 641012-0003.